Cell Stem Cell
Article

Genome-wide Chromatin Interactions of the *Nanog* Locus in Pluripotency, Differentiation, and Reprogramming

Effie Apostolou,[1,2,3,11] Francesco Ferrari,[4,11] Ryan M. Walsh,[1,2,3] Ori Bar-Nur,[1,2,3] Matthias Stadtfeld,[1,2,3,9] Sihem Cheloufi,[1,2,3] Hannah T. Stuart,[1,2,3] Jose M. Polo,[1,2,3,10] Toshiro K. Ohsumi,[5] Mark L. Borowsky,[5] Peter V. Kharchenko,[4,6] Peter J. Park,[4,7,8,*] and Konrad Hochedlinger[1,2,3,*]
[1]Massachusetts General Hospital Cancer Center and Center for Regenerative Medicine, 185 Cambridge Street, Boston, MA 02114, USA
[2]Harvard Stem Cell Institute, 1350 Massachusetts Avenue, Cambridge, MA 02138, USA
[3]Howard Hughes Medical Institute and Department of Stem Cell and Regenerative Biology, Harvard University and Harvard Medical School, 7 Divinity Avenue, Cambridge, MA 02138, USA
[4]Center for Biomedical Informatics, Harvard Medical School, 10 Shattuck Street, Boston, MA 02115, USA
[5]Department of Molecular Biology, Massachusetts General Hospital and Harvard Medical School, 185 Cambridge Street, Boston, MA 02114, USA
[6]Division of Hematology/Oncology
[7]Informatics Program
Children's Hospital, Boston, MA 02115, USA
[8]Division of Genetics, Brigham and Women's Hospital, Boston, MA 02115, USA
[9]Present address: The Helen L. and Martin S. Kimmel Center for Biology and Medicine, The Skirball Institute of Biomolecular Medicine, New York University, New York, NY 10016, USA
[10]Present address: Australian Regenerative Medicine Institute and Department of Anatomy and Developmental Biology, Monash University, Wellington Rd, Clayton, Vic 3800, Australia
[11]These authors contributed equally to this work
*Correspondence: peter_park@harvard.edu (P.J.P.), khochedlinger@helix.mgh.harvard.edu (K.H.)
http://dx.doi.org/10.1016/j.stem.2013.04.013

SUMMARY

The chromatin state of pluripotency genes has been studied extensively in embryonic stem cells (ESCs) and differentiated cells, but their potential interactions with other parts of the genome remain largely unexplored. Here, we identified a genome-wide, pluripotency-specific interaction network around the *Nanog* promoter by adapting circular chromosome conformation capture sequencing. This network was rearranged during differentiation and restored in induced pluripotent stem cells. A large fraction of *Nanog*-interacting loci were bound by Mediator or cohesin in pluripotent cells. Depletion of these proteins from ESCs resulted in a disruption of contacts and the acquisition of a differentiation-specific interaction pattern prior to obvious transcriptional and phenotypic changes. Similarly, the establishment of *Nanog* interactions during reprogramming often preceded transcriptional upregulation of associated genes, suggesting a causative link. Our results document a complex, pluripotency-specific chromatin "interactome" for *Nanog* and suggest a functional role for long-range genomic interactions in the maintenance and induction of pluripotency.

INTRODUCTION

Three-dimensional (3D) chromatin architecture is important for many biological processes including transcriptional regulation. For example, looping between promoter and enhancer or insulator elements controls the transcriptional activation or repression of genes, respectively (Engel and Tanimoto, 2000; Ling et al., 2006; Zhao et al., 2006). Although long-range chromatin interactions have been observed mostly in *cis* along the same chromosome (Schoenfelder et al., 2010), they can also occur in *trans* between different chromosomes. Interactions in *trans* are associated with coregulation of imprinted genes (Zhao et al., 2006) or genes associated with erythropoiesis (Schoenfelder et al., 2010), with stochastic selection for monoallelic activation of the *IFN-β* locus (Apostolou and Thanos, 2008) and olfactory genes (Clowney et al., 2012; Lomvardas et al., 2006), and with activation-induced cytidine deaminase-mediated translocations (Klein et al., 2011; Rocha et al., 2012). Although the organization of chromosomes into defined territories was reported three decades ago (Schardin et al., 1985), the molecular principles of global chromatin architecture have only recently been explored with high-throughput technologies such as the Hi-C method (Dixon et al., 2012; Duan et al., 2010; Lieberman-Aiden et al., 2009; Sexton et al., 2012; Zhang et al., 2012).

Chromatin organization also plays a role in the control of pluripotency and cellular differentiation. For instance, pluripotency-associated genes such as *Sox2*, *Nanog*, and *Klf4* relocate from the nuclear center to the nuclear periphery upon differentiation of mouse embryonic stem cells (ESCs) (Peric-Hupkes et al., 2010). Moreover, the loss of promoter-enhancer interactions at key pluripotency genes, including *Nanog* and *Oct4*, during ESC differentiation has been associated with silencing of these genes (Kagey et al., 2010; Levasseur et al., 2008). Proteins involved in chromatin looping, including CTCF, cohesin, and Mediator, co-occupy many genomic targets of pluripotency factors (Kagey et al., 2010; Nitzsche et al., 2011) or directly interact with them

(Donohoe et al., 2009; Tutter et al., 2009). These molecules might therefore cooperate to arrange a higher-order chromatin structure that maintains pluripotency. Indeed, depletion of Mediator and cohesin subunits from ESCs results in unscheduled differentiation (Kagey et al., 2010). A more recent study using the Hi-C technology in mouse and human ESCs and differentiated cells identified a network of local chromatin-interaction domains, so-called topological domains, with conserved boundaries among different species and cell types (Dixon et al., 2012). Although that report documented important general principles of chromatin organization in pluripotent and differentiated cells, a high-resolution map of genome-wide interactions of pluripotency genes in ESCs is lacking. It also remains unclear which molecules might be involved in establishing such putative connections, and whether and how these patterns change upon differentiation.

Forced expression of the transcription factors Oct4, Sox2, Klf4, and c-Myc is sufficient for endowing somatic cells with pluripotency, giving rise to induced pluripotent stem cells (iPSCs) (Takahashi and Yamanaka, 2006). In-depth molecular analysis of reprogramming intermediates has been achieved only recently with improved technologies for studying rare and defined cell populations (Buganim et al., 2012; Golipour et al., 2012; Polo et al., 2012; Soufi et al., 2012). In addition, molecular characterization of stable partially reprogrammed iPSC (piPSC) lines sheds light on the earliest events in cellular reprogramming (Mikkelsen et al., 2008; Sridharan et al., 2009). Although these studies reported the reestablishment of an ESC-like transcriptional and epigenetic state, it remains unclear whether, when, and how the 3D chromatin structure is reset during cellular reprogramming into iPSCs.

In this study, we have investigated the genome-wide interaction network of the *Nanog* gene, which is indispensable for development as well as for the derivation of ESCs (Mitsui et al., 2003; Chambers et al., 2003) and iPSCs (Silva et al., 2009). We developed a modified version of circular chromosome conformation capture sequencing (m4C-seq) to determine the genome-wide interaction partners of the *Nanog* locus in ESCs, iPSCs, and mouse embryonic fibroblasts (MEFs) at high resolution. Our study provides the first detailed chromatin-interaction map of a key pluripotency locus on a genomic scale and offers mechanistic insights into the regulation of chromatin architecture during the acquisition and maintenance of pluripotency.

RESULTS

The *Nanog* Locus Engages in Distinct Genome-wide Interactions in Pluripotent and Differentiated Cells

We developed a modified version of 4C-seq for unbiased genome-wide capture of *Nanog*'s interactions in pluripotent and differentiated cells (Figure 1A; see Experimental Procedures). In brief, 4C technology is based on the proximity-ligation principle, in which unknown chromatin loci that interact with a known "bait" locus (e.g., *Nanog*) are ligated into chimeric DNA molecules and then identified by deep sequencing (Dekker et al., 2002). m4C-seq involves ligation of universal adapters to the linearized hybrid molecules, followed by ligation-mediated PCR with an adaptor-specific oligonucleotide and a biotinylated primer recognizing the *Nanog* locus. This allows specific enrichment and purification of the *Nanog*-interacting regions using streptavidin beads and avoids the less-efficient recircularization and inverse-PCR steps of published 4C methods.

To increase confidence in observed interactions, we used biological replicates, applied multiple filtering and normalization steps, and adjusted for random ligation events and possible technical biases based on a control sample (noncrosslinked genomic DNA; see Experimental Procedures). Technical replicates generated by independent ligation, amplification, and sequencing showed a high level of concordance (Spearman's rank correlation coefficient $\approx$ 0.9) (Figure S1A available online). We then analyzed three independent biological replicates for ESC lines (R1, V6.5, and KH2-ESC1), MEFs, and fibroblast-derived iPSC clones previously shown to give rise to entirely iPSC-derived mice, thus satisfying the most stringent criteria of pluripotency (Stadtfeld et al., 2010a). The biological replicates of pluripotent cells showed higher variability than the technical replicates, as expected, but nevertheless exhibited high correlation (Spearman's coefficient $\approx$ 0.7) (Figures S1A–S1D). However, MEF replicates showed notably lower correlation (Spearman's coefficient $\approx$ 0.3), suggesting that *Nanog* may have less-stable interactions in MEFs, perhaps because the gene is not active.

Unsupervised clustering (Figure 1B) highlighted similarities between ESCs and iPSCs, which clustered separately from MEFs. Consistent with this observation, we found extensive overlap ($\sim$70%) among the conserved *Nanog* interactions in ESCs and iPSCs (Table S1), but much less overlap between these pluripotent samples and MEFs (<10% of pluripotent interactions) (Figure 1C). The higher variability in MEF samples resulted in a smaller set of conserved interactions among replicates (Figures 1C and S1C; Table S1). These results show distinct *Nanog* interactomes in differentiated and pluripotent cells.

Given that *Nanog* is located in a gene-rich genomic region containing other pluripotency loci, we first examined a 200 kb window around its promoter. We detected several interaction partners, including the *Nanog* enhancer, *Aicda*, *Apobec1*, and *Scl2a3* genes (Figure S1E). We obtained reads for 11 out of 12 loci that have previously been tested in ESCs by chromosome conformation capture (3C) (Levasseur et al., 2008). We also identified broad interaction domains in distal regions on chromosome 6, visualized in the form of a "domainogram" (Figure S2A) (Bantignies et al., 2011). Randomly selected interactions within the broad domains were verified by 3D DNA fluorescence in situ hybridization (FISH) (Figures 1D, 1E, and S2B) and by 3C analysis among single HindIII fragments using independent cell preparations (Figure S2D). FISH results were independently confirmed for a subset of nuclei ($\sim$250 nuclei for three probes in total) at a higher resolution, which allowed for more accurate measurement of colocalized signals (<250 nm, Figure S2C).

Broad interaction domains with differential strengths in ESCs and MEFs are shown in Figure 1F. MEF-derived iPSCs and ESCs showed similar differential domainogram patterns when compared to MEFs, suggesting that reprogramming restored the ESC-specific 3D structure along chromosome 6. Furthermore, *cis* interaction patterns observed in published Hi-C data for ESCs (Dixon et al., 2012) exhibited a higher correlation to those we detected in ESCs and iPSCs than to those in MEFs (Figure S2E). Together, these data document that *Nanog* forms a pluripotency-specific interactome with multiple genomic regions along its entire chromosome in both ESCs and iPSCs.

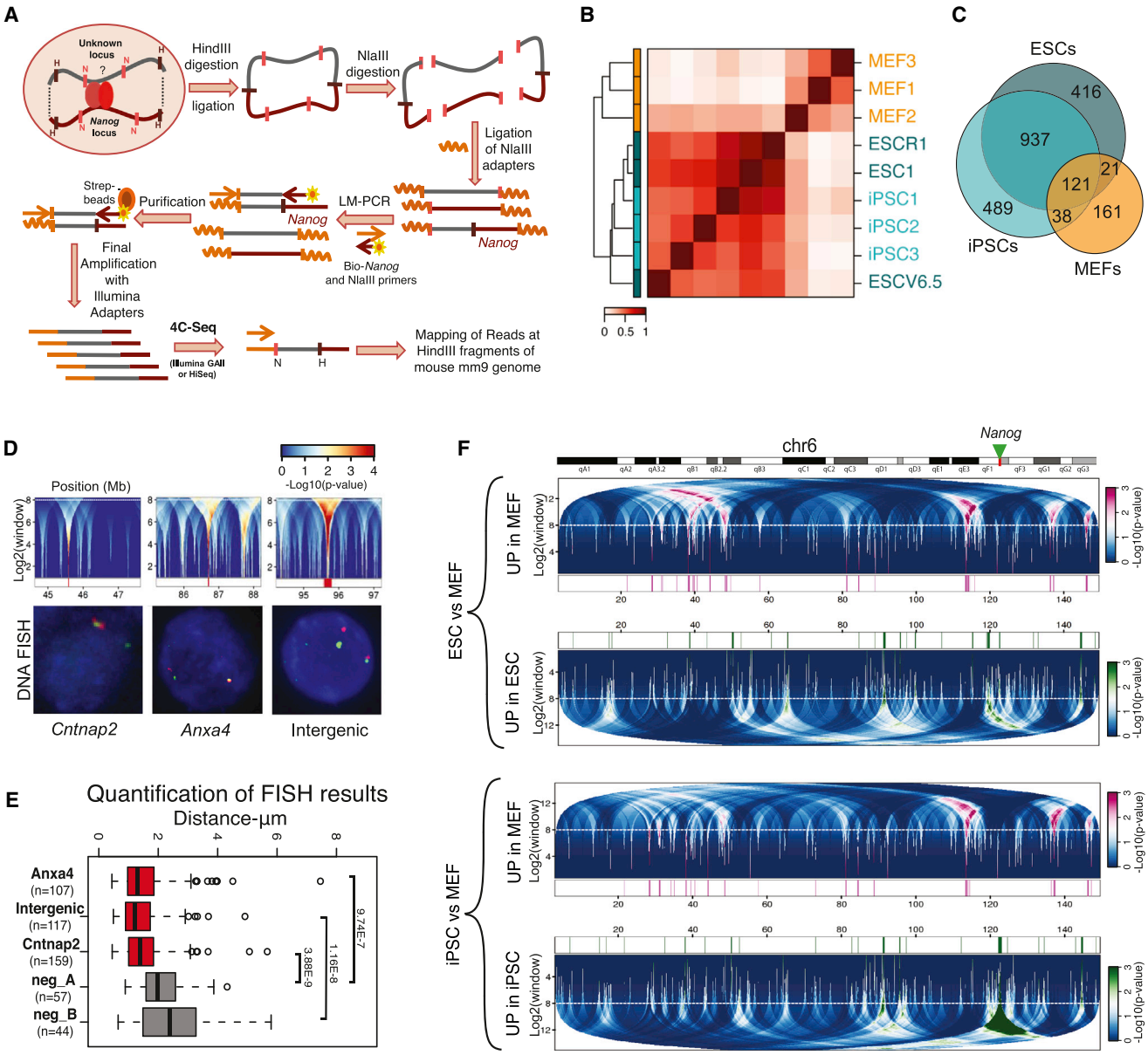

Figure 1. Genome-wide Interactions of the *Nanog* Locus in Differentiated and Pluripotent Cells

(A) Schematic representation of m4C-seq. LM-PCR, ligation-mediated PCR; Strep-beads, streptavidin-conjugated beads; H, HindIII site; N, NlaIII site.

(B) Unsupervised clustering and correlation matrix of pluripotent and differentiated cells (three ESCs, three iPSCs, and three MEFs). Normalized (observed over expected) m4C-seq signals at individual HindIII fragments are clustered, with Spearman's correlation (color gradient) and average linkage shown. Fragments detected in at least three out of nine samples are used.

(C) Venn diagram showing the degree of overlap among the *Nanog*-interacting HindIII fragments common within each group: ESCs, iPSCs, and MEFs.

(D) The upper panels show details of domainogram analysis for broad intrachromosomal interaction domains (*Cntnap2*, *Anxa4*, and an intergenic region) in individual samples. Regions around broad interaction domains are shown for a representative ESC sample (ESC1 cell line). The centers of interacting domains are marked in red at the bottom (p value < 0.0001). The dashed horizontal white line indicates the maximum-window-size cutoff. The bottom panels show representative 3D DNA FISH in ESCs confirming the interaction of *Nanog* (green fluorescein isothiocyanate [FITC] signals) with each of those domains (magenta Alexa 568 signals).

(E) Boxplot for distances between the *Nanog* locus and the tested domains (n = number of measured nuclei). Intrachromosomal regions between the positive hits and the bait position were used as negative controls (neg_A and neg_B). p values for the Wilcoxon signed-rank test are reported (see also Figure S2C). Whiskers extend to the most extreme values within 1.5 times the interquartile range from the upper or lower quartile.

(F) Differential interactions over large domains (domainogram) for ESCs versus MEFs (upper panel) and iPSCs versus MEFs (bottom panel) on chromosome 6. The green arrow indicates the *Nanog* position. Top: interacting domains upregulated in MEFs (magenta); bottom: interacting domains upregulated in ESCs or iPSCs, respectively (green). In the central part, magenta and green marks indicate the regions significantly upregulated (p value < 0.001) in MEFs and ESCs or iPSCs, respectively. The dashed horizontal white line indicates the maximum-window-size cutoff. All replicates for each cell type are taken into account for computing the score for differential interactions.

See also Figures S1 and S2 and Tables S1 and S6.

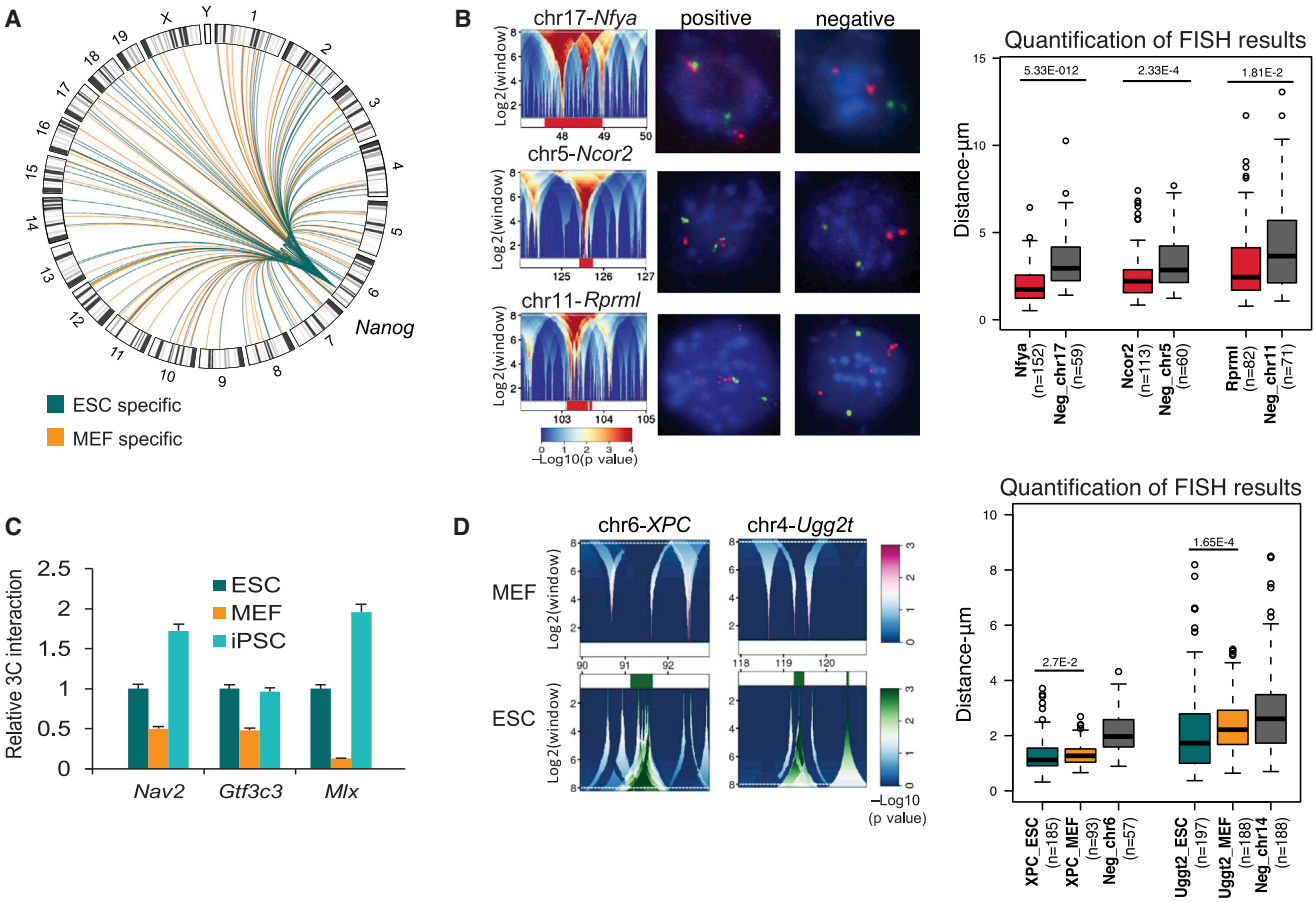

Figure 2. Detection and Validation of Interchromosomal Associations of the *Nanog* Locus in Pluripotent and Differentiated Cells

(A) Circos plot for differential interchromosomal interactions in ESCs (green) compared to MEFs (orange) as detected from broad domain analysis using domainograms (Figure 1F) in each chromosome.

(B) Three interchromosomal *Nanog*-interacting domains confirmed by 3D DNA FISH in ESCs. The domainograms refer to the ESC1 line and are representative of other ESCs. Representative 3D DNA FISH images show the *Nanog* alleles (green FITC signals) interacting with each of those domains (left) or their corresponding negative controls (right) (magenta Alexa 568 signals). The boxplots report 3D DNA FISH results (n = number of nuclei; p = Wilcoxon test p value) (whiskers are as in Figure 1E). Negative controls were selected in regions within 2 Mb of the targets.

(C) 3C PCR confirmation of selected differential interchromosomal interactions of the *Nanog* locus in ESCs and iPSCs versus MEFs. For each primer pair, the PCR signal was calculated relative to the corresponding signal in ESCs ("Relative 3C Interaction") after normalization with the PCR signal of primers designed at the bait locus (see Table S6). Error bars indicate SD (n = 3 technical replicates). All 3C PCR products were isolated and analyzed by Sanger sequencing.

(D) Domainogram details for differential interactions around *XPC* and *Ugg2t*, which were found to interact with *Nanog* preferentially in ESCs. Top (magenta) and bottom panels (green) refer to interaction enrichment in MEFs and pluripotent cells, respectively. 3D DNA FISH results for the two regions are shown in the boxplot, similarly to (B) (whiskers are as in Figure 1E).

See also Figure S2 and Tables S2 and S6.

Nanog Participates in Pluripotency-Specific Interchromosomal Associations

Many of the detected contacts were found to be *trans* interactions of *Nanog* with other chromosomes (Figure 2A and Table S1). Although previous studies using conventional 4C-seq protocols did not detect such a high number of *trans* associations (Simonis et al., 2006, 2009), our results are consistent with a similar 4C adaption termed "enhanced 4C" (e4C) (Schoenfelder et al., 2010). We believe that m4C-seq and e4C approaches using universal adapters and streptavidin-based purification and enrichment of the bait locus enable greater sensitivity. The high number of observed interchromosomal interactions is further supported by the tendency of the *Nanog* locus to localize on the edge or outside of its chromosome territory (Figure S2F). Moreover, reanalysis of recently published Hi-C data from mouse ESCs (Dixon et al., 2012) showed that over 60% of *Nanog*'s *trans* interactions overlapped significantly with our m4C-seq interactions in ESCs and iPSCs, but not with those in MEFs (Figure S2G). Selected interacting regions in ESCs, localized on three different chromosomes, were tested by 3D DNA FISH in ESCs, and they showed closer proximity to the *Nanog* locus compared with noninteracting regions on the respective chromosomes (Figure 2B).

The distribution of broad differential intra- and interchromosomal interaction domains in pluripotent (ESCs) versus differentiated (MEFs) cells is visualized in Figure 2A. In addition,

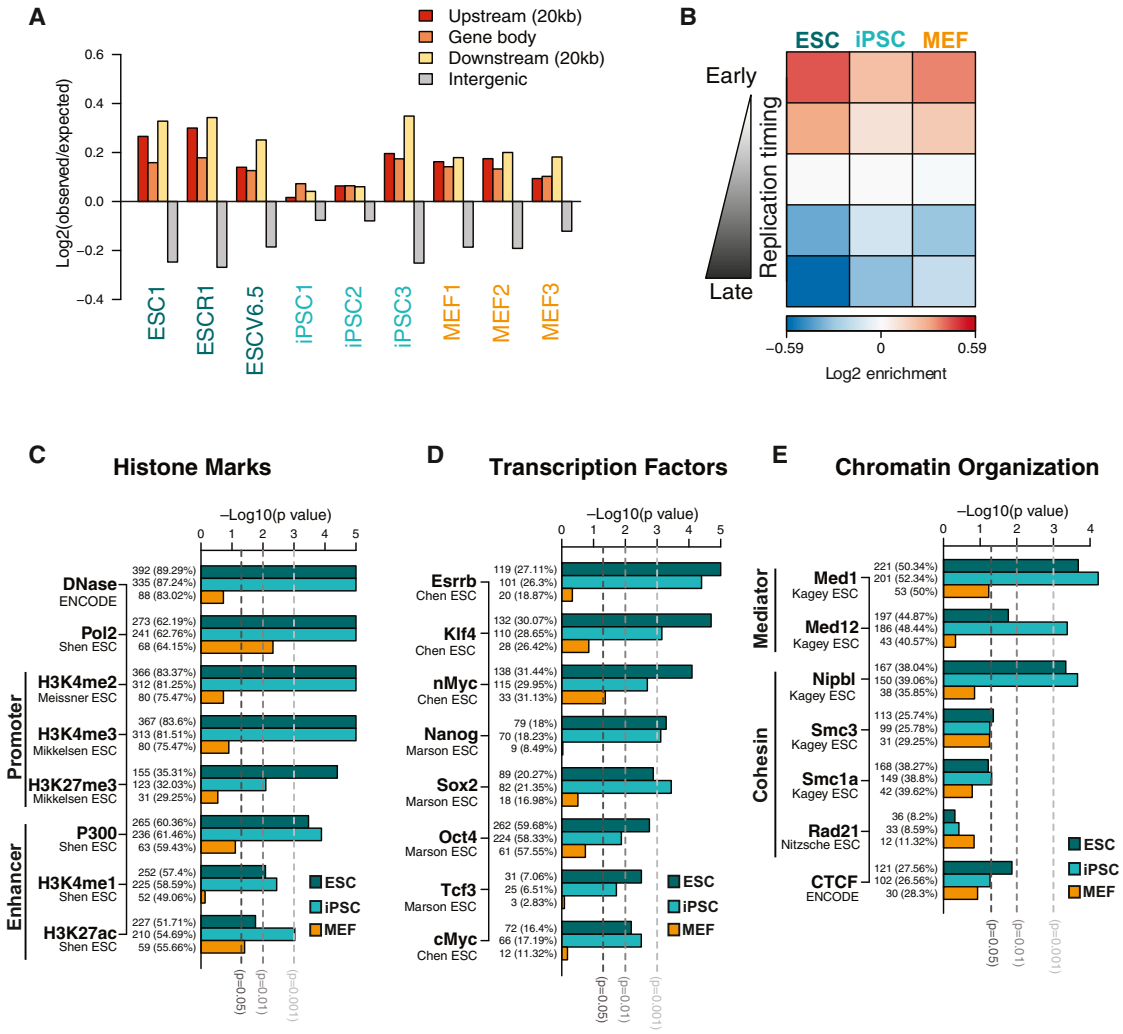

Figure 3. *Nanog*-Interacting Regions Are Enriched for Open Chromatin Features and Pluripotency-Factor Binding in Pluripotent Cells

(A) Distribution of the *Nanog*-interacting loci detected at single-fragment level in each sample. Log ratios of observed over expected fragments in different genomic regions show a consistent overrepresentation of interactions in genes and surrounding regions (20 kb upstream or downstream).

(B) Association of the *Nanog*-interacting regions with replication timing (RT). Genomic segments were divided into five groups (from early to late) based on their RT data in each cell type (Hiratani et al., 2010). The median association of interacting fragments (observed over expected log ratio) across biological replicates is plotted as a heatmap.

(C) Association of conserved *Nanog* interactions within each cell type (ESCs, iPSCs, or MEFs) with active or repressive chromatin features. Conserved *Nanog* interactions were identified by gene-level analysis; ChIP peaks in ESCs were linked to genes when overlapping with a −5 kb-to-+1 kb window at transcriptional start sites. The barplots show the significance of association between *Nanog*-interacting genes and genes enriched for a given mark, tested independently for each cell type. The number and the percentage of interacting genes with a given chromatin mark are reported for each bar.

(D and E) Similar analyses of association to genes bound by pluripotency transcription factors in ESCs (D) and genes bound by components of cohesin and Mediator complexes and CTCF in ESCs (E) are shown.

See also Figure S3 and Table S3.

differential interactions selected at the single-fragment level are reported in Table S2 and shown in Figure S1B. We confirmed several of the differential interactions between MEFs and ESCs, either by 3C (Figure 2C) or 3D DNA FISH analysis (Figure 2D) using independent cell preparations. Collectively, these results show that *Nanog* forms a complex genomic interaction network with multiple chromosomes that differs between pluripotent and differentiated cells and is restored in iPSCs.

Nanog-Interacting Loci Are Enriched for Open Chromatin Features as well as Binding Sites for Pluripotency Factors, Cohesin, and Mediator

To determine whether *Nanog*-interacting loci share common genomic features, we compared our results with published data (Table S3). We first noticed consistent enrichment for gene bodies and surrounding regulatory regions among interactions in ESCs, iPSCs, and MEFs (Figure 3A), as well as for early-replicating domains, which typically exhibit an open

chromatin structure (Figure 3B). The latter correlation is consistent with the fact that *Nanog* replicates early in both cell types despite its transcriptional silencing in MEFs (Hiratani et al., 2008, 2010).

We next examined chromatin features of pluripotent cells including histone marks (Table S3) and DNase I hypersensitivity among *Nanog*-interacting genes using data from the Encyclopedia of DNA Elements project (ENCODE Project Consortium, 2011). *Nanog*-interacting genes in pluripotent cells were enriched for the activating histone marks H3K4me3 and H3K4me2 and enhancer marks (H3K27ac, H3K4me1, and p300), as well as for DNase I-hypersensitive sites characterizing open chromatin areas (Figures 3C and S3A). A weak correlation was also detected for the repressive H3K27me3 mark and for bivalent promoters (p value < 0.05 in ESCs and iPSCs). However, we were unable to detect significant and consistent enrichment for binding sites of the Polycomb complex, which deposits H3K27me3 (Figures 3C and S3A). Thus, *Nanog* interacts mostly with active genes and regulatory elements in pluripotent cells.

To gain mechanistic insights into how the identified interactions are established, we searched for enrichment of pluripotency transcription factor binding sites among the *Nanog*-interacting loci using published chromatin immunoprecipitation sequencing (ChIP-seq) data sets (Table S3). Indeed, target sites for Esrrb, Klf4, c-Myc, and Sox2 were among the most consistently and significantly enriched sequences, whereas enrichment of Nanog and Oct4 targets varied across data sets (Figures 3D and S3B). We also found a pluripotency-specific association with binding of additional factors of the pluripotency network (Chen et al., 2008), including Tcf3, Tcfcp2l1, Nr5a2, and Zfx (Figures 3D and S3B). Together, these data show that genes interacting with *Nanog* in ESCs and iPSCs are strongly enriched for binding of essential pluripotency factors. It remains to be tested whether this result reflects that coregulated genes are spatially connected or that some of these factors are actively involved in chromatin looping.

We also examined occupancy of cohesin, Mediator, and CTCF molecules, proteins reported to mediate long-range interactions, among the ESC-specific contacts (Table S3). We found a significant association of *Nanog* interactions in pluripotent cells with binding of the Mediator (Med1 and Med12) and cohesin (Smc1a, Nipbl, and Smc3) complexes and a less-consistent correlation with CTCF binding depending on the data set (Figures 3E and S3C). Collectively, these results suggest that key pluripotency transcription factors might collaborate with molecules known to mediate promoter-enhancer looping and general chromatin organization to establish the observed pluripotency-specific *Nanog* interactome.

Nanog Interactions Are Dependent on Mediator and Cohesin Subunits in ESCs

We next asked how many of those regions were indeed bound by the Mediator and cohesin complexes in ESCs. To this end, we performed "4C-ChIP-seq" (Figure 4A), wherein ChIP for the Med1 and Smc1 proteins was carried out before sequencing of the *Nanog*-centered m4C libraries (Figure S4A and Experimental Procedures). Loci bound by Med1, Smc1, or both accounted for about 40% of all ESC-specific interactions (Figure 4B; Table S4). These data reinforce the results of our association analysis with published data and show that a large portion of the ESC-specific *Nanog* interactions involve the Mediator and cohesin complexes.

To test whether *Nanog* interactions require the Mediator or the cohesin complex, we performed m4C-seq in ESCs transduced with lentiviral vectors expressing short hairpin RNAs (shRNAs) against *Smc1a* or *Med1* (Figures 4A and S4B; Table S6). Chromatin was isolated 5 days after viral transduction, when protein levels were substantially reduced (Figure S4B) but before the onset of differentiation, as assessed by their undifferentiated morphology (Figure S4C) and the ESC-like messenger RNA (mRNA) and protein levels of several pluripotency factors (Figures 4C, S4D, and S4E). Importantly, *Nanog*'s promoter-enhancer interaction was already disrupted at day 5 of *Med1* or *Smc1a* knockdown (KD) (Figure 4D), although *Nanog* transcription was still detectable by RT-PCR (Figure 4C) and by the presence of Pol II phospho-Ser2 on the *Nanog* promoter (Figure S4F). Med1- and Smc1a-mediated *Nanog* interactions were severely reduced or completely abrogated in the day 5 KD 4C-seq samples (Figure 4E). Loss of chromatin contacts was confirmed by DNA FISH for one of the interacting candidate loci (Figure 4F). RNA sequencing (RNA-seq) analysis of *Med1* and *Smc1a* KD ESCs confirmed downregulation of pluripotency-related genes and upregulation of differentiation-related genes by day 8, whereas these changes were less evident on day 5 (Figure S4G). The altered transcriptional profiles of our KD cells at day 8 resembled those of previously published ESCs infected with shRNAs against *Med12* (another Mediator subunit) or *Smc1a* (Kagey et al., 2010) (Figure S4H). The faster kinetics of differentiation upon *Med12* and *Smc1a* KD reported in that study probably resulted from a more efficient depletion with a different vector system. Remarkably, the m4C-seq profiles of KD ESCs indicated that the majority of the ESC-specific interactions were lost (Figures 4H and S4I), whereas many of the MEF-specific interactions were established, presumably in a Med1- or Smc1a-independent manner (Figures 4G and 4H). Thus, Smc1a and Med1 depletion led to rearrangement of chromatin from a pluripotent- to a differentiation-specific state, even though cells still showed phenotypic and transcriptional features of the pluripotent state.

The *Nanog* Interactome Undergoes Dramatic Changes during Somatic Cell Reprogramming

Given that iPSCs have reset the *Nanog* interactome from a somatic to a pluripotent state, we assessed when chromatin rearrangements occur during reprogramming and how these relate to gene-expression changes. Specifically, we compared the kinetics of chromatin looping with gene expression using piPSC lines and sorted SSEA1$^+$ intermediates at different stages of reprogramming (Figure 5A). Importantly, both piPSCs and SSEA1$^+$ intermediates have exited the somatic state and are poised to form iPSCs under different conditions, consistent with previous observations (Figures S5A and S5B) (Sridharan et al., 2009; Stadtfeld et al., 2008). In further agreement with those previous reports, we found that *Nanog* is not yet expressed in piPSCs, whereas it is gradually upregulated during mid-to-late stages of reprogramming (Figure 5B). Surprisingly, 3C analysis revealed that looping between the *Nanog* enhancer

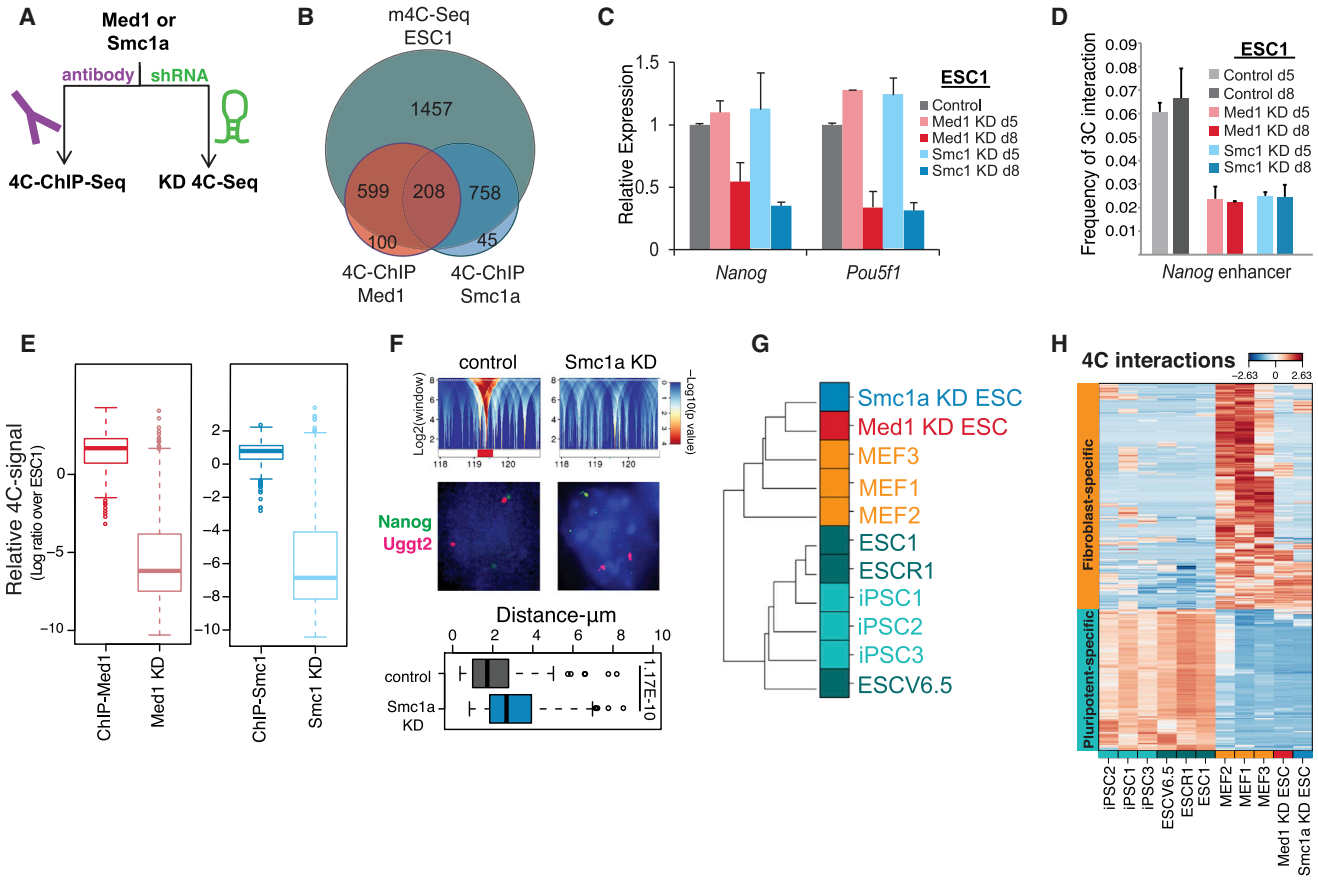

Figure 4. Mediator and Cohesin Coordinate *Nanog*'s Genomic Interactions in Pluripotent Cells

(A) Two-pronged strategy for testing the role of candidate proteins in the *Nanog* interactome in ESCs.

(B) Venn diagram depicting the overlap of *Nanog*-interacting HindIII fragments detected by m4C-ChIP-seq for either Med1 or Smc1a compared to m4C-seq in ESC line ESC1.

(C) RT-PCR analysis for pluripotency genes *Nanog* and *Pou5f1* in ESCs treated with shRNAs against *Med1* or *Smc1* for 5 (d5) or 8 days (d8). Error bars indicate SD (n = 3 technical replicates). m4C-seq analysis was performed on day 5, before downregulation of *Nanog* or *Pou5f1* and apparent differentiation of cells.

(D) 3C PCR quantifying the interaction frequency between the *Nanog* promoter and enhancer in control ESCs and in ESCs harvested 5 (d5) or 8 days (d8) after knocking down Med1 or Smc1a. For each primer pair, the PCR signal was normalized to the PCR signal of primers designed at the bait locus (see Table S6). Error bars indicate SD (n = 3 technical replicates).

(E) Boxplot reporting the relative change in 4C-seq normalized signal of the 4C-ChIP selected fragments compared to ESC1 (log2 ratio) (whiskers are as in Figure 1E).

(F) Top: domainogram details showing the interaction of *Nanog* with the *Uggt2* locus in control ESC1 and its disruption in Smc1a KD ESC1. Middle: representative DNA FISH photos for *Nanog* (FITC signal) and *Uggt2* (magenta signal) in control or *Smc1a* KD ESCs. Bottom: boxplot for distances between the *Nanog* and *Ugg2t* as measured by DNA FISH (whiskers are as in Figure 1E). The difference is significant (Wilcoxon test).

(G) Unsupervised clustering of samples is performed as in Figure 1B with the addition of the ESC samples for *Med1* or *Smc1a* KD.

(H) Heatmap showing the relative change in m4C-seq signal for the set of 4C fragments selected as differential interactions between ESCs and MEFs, clearly showing that the pluripotency-specific interactions have been lost in the *Med1* or *Smc1a* KD sample. The rows refer to individual HindIII fragments, and the columns are different 4C-seq samples. The color refers to standardized values across samples (*Z* score) for log-transformed normalized 4C read counts.

See also Figure S4 and Tables S4 and S6.

and promoter was established in both piPSC and in SSEA1$^+$ intermediates before detectable transcriptional activation of *Nanog* (Figure 5C). We extended this analysis by performing 3C analysis in piPSCs for *Oct4*, *Phc1* and *Lefty1,* which form promoter-enhancer loops in ESCs (Figure S5C) (Kagey et al., 2010). Whereas *Phc1* already exhibited looping and expression in piPSCs, *Oct4* had neither initiated looping nor activated expression. In contrast, *Lefty1* had initiated looping, but not yet expression, akin to the *Nanog* locus. These results support the conclusion that the looping at the examined pluripotency-associated genes precedes, but is not sufficient for, transcriptional activation in the context of cellular reprogramming.

On a genome-wide scale, m4C-seq analysis of piPSCs and SSEA1$^+$ intermediates showed that both cell populations had lost a large fraction of the MEF-specific interactions and had gained a small number of ESC-specific interactions (Figures 5D, S5D, and S5E). Unexpectedly, we also observed a number of reprogramming-specific interactions detectable neither in MEFs nor in iPSCs (Table S5). Transient interactions were variable among SSEA1$^+$ samples from independent reprogramming

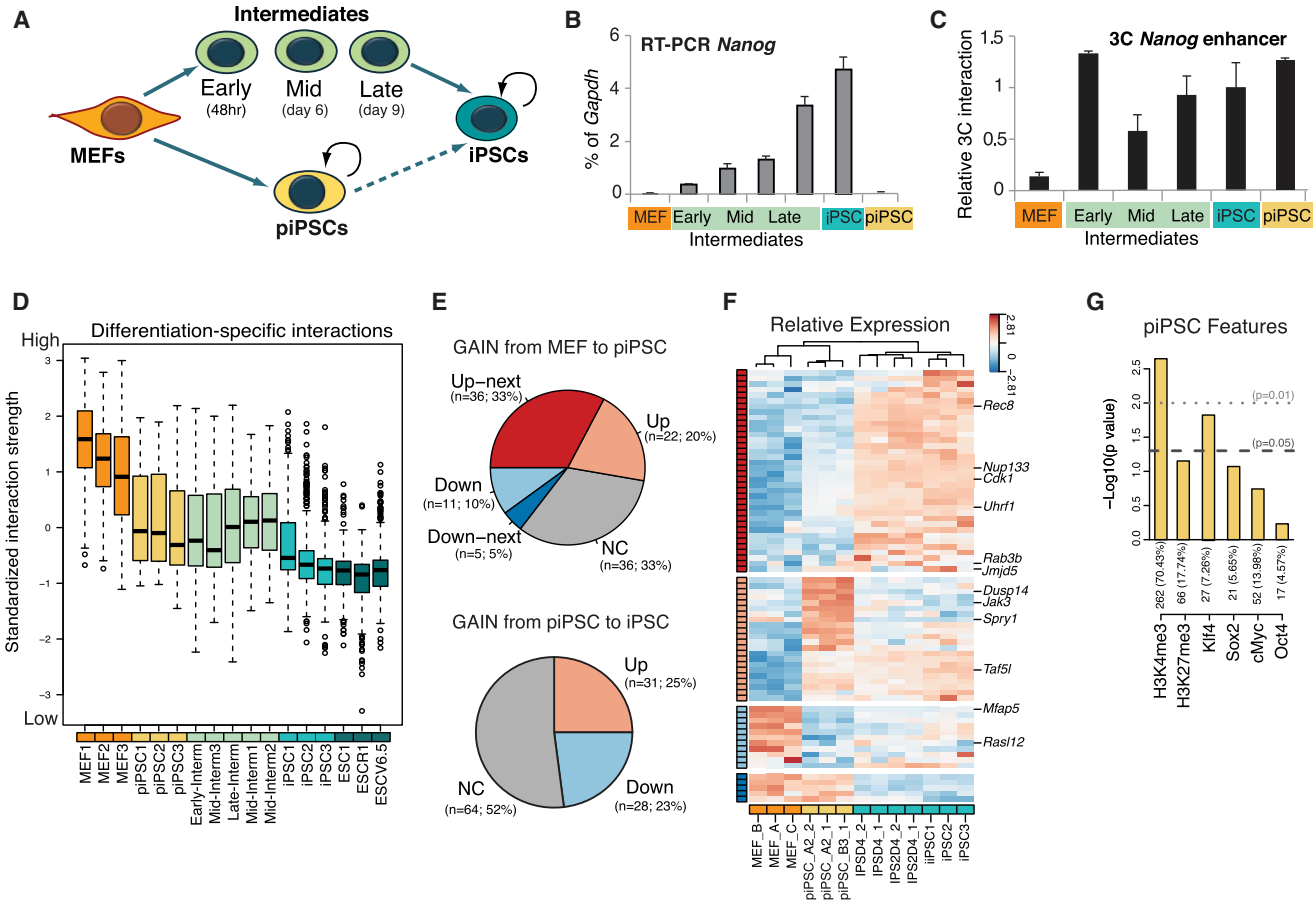

Figure 5. Dynamic Change of *Nanog* Interactome during Cellular Reprogramming into iPSCs

(A) Isolation and study of reprogramming intermediates and piPSCs.

(B) RT-PCR analysis for *Nanog* mRNA in indicated cell populations. The *Nanog* expression is normalized over *Gapdh* (% of *Gapdh*). The error bars indicate SD (n = 3 technical replicates). Late intermediates include SSEA1$^+$ cells from day 9 and day 12.

(C) 3C analysis of relative interaction frequency between the *Nanog* promoter and enhancer during reprogramming and in the piPSCs. The PCR signal is relative to ESCs ("Relative 3C Interaction") after normalization with bait-locus primers (see Table S6). Error bars represent SD (n = 3 technical replicates).

(D) Boxplot for the standardized interaction strength for differentiation-specific fragments (whiskers are as in Figure 1E). The fragments were selected as differential fragments upregulated in MEFs versus ESCs. Five groups of samples are shown: ESCs, iPSCs, SSEA1$^+$ intermediates, piPSCs, and MEFs. SSEA1 intermediates and piPSCs show an intermediate interaction strength between stronger MEFs and weaker ESCs and iPSCs. For each fragment, the log-transformed normalized 4C read counts are standardized by subtracting the mean value across all samples, then dividing over SD (*Z* score) (see also Figure S5D).

(E) Pie charts showing the number of genes, which have established (gain) interactions with *Nanog* during the transition from MEFs to piPSCs (upper panel) or from piPSCs to iPSCs (lower panel). Genes are grouped based on the change of expression detected by microarray data (false discovery rate = 0.05; fold change = 1.3) (Sridharan and Hochedlinger data sets, Table S3 and Figure S5G). Up/Down, up-/downregulated genes in the transition from MEFs to piPSCs (upper panel) or from piSPCs to iPSCs (lower panel); Up-/Down-next (for the upper panel only), represents up-/downregulated genes in the next stage, i.e., the transition from piPSCs to iPSCs (see also F); NC, genes without a statistically significant change in expression. The number of genes and percentage over the total are indicated. We found significant enrichment in the "Up-next" group (one-tailed Fisher's exact test, p = 0.001). Gene-level interactions detected in all piPSC replicates and in none of the MEFs were used.

(F) Heatmap showing expression of *Nanog*-interacting genes gained in the MEF-to-piPSC transition, as in (E). Rows are genes, and columns are microarray samples (Table S3). Expression-pattern groups were defined as in (E) and marked accordingly with the side color bar. Some genes showed significant upregulation in both the MEF-to-piPSC and the piPSC-to-iPSC transitions. In this case, they were assigned to the "Up-next" group as well. The statistically significant enrichment in the "Up-next" pattern is confirmed even if these genes are assigned to the "Up" group. The heatmap shows standardized gene-expression levels across samples (*Z* score).

(G) Association of conserved *Nanog*-interacting genes in piPSCs with H3K4me3, H3K27me3, and pluripotency transcription factors binding in the same cell type. The number and percentage of interacting genes with ChIP enrichment is reported for each bar. The analysis criteria is similar to that in Figure 3.

See also Figure S5 and Table S5.

experiments, probably reflecting their heterogeneity (see single-cell RT-PCR of Figure S5F and Polo et al., 2012). We therefore focused on piPSCs, which are of clonal origin and hence more homogeneous. Notably, these transient interactions in piPSCs (Table S5) were preferentially associated with pluripotency- rather than differentiation-related genes (p value = 0.014). Thus, forced expression of reprogramming factors readily extinguished fibroblast-specific interactions and induced a large

number of transient chromatin interactions enriched for pluripotency-associated genes.

We next correlated the reorganization of *Nanog*'s interactome during reprogramming with transcriptional changes of associated genes. Notably, more than 50% of genes that established interactions with *Nanog* during the transition of MEFs into piPSCs became transcriptionally upregulated in piPSCs ("Up") or at the subsequent (iPSC) stage ("Up-next") (Figures 5E, 5F, and S5G). These results extend, to a genome-wide level, our previous observations that the gain of *Nanog*-centered chromatin contacts during early reprogramming coincides with or precedes transcriptional changes of genes. Unexpectedly, the interactions gained during the piPSC-to-iPSC transition showed a weaker correlation with transcriptional changes, suggesting a lesser impact of *Nanog* interactions on gene expression during the late stages of reprogramming. We conclude that *Nanog*'s chromatin associations during early stages of reprogramming mostly involve genes that are either immediately upregulated or poised for activation in iPSCs.

To investigate which molecules might mediate *Nanog*'s interactions during reprogramming, we compared m4C-seq results on piPSCs with published ChIP-chip data of reprogramming factors and histone modifications in the same cell type (Sridharan et al., 2009). This analysis revealed a positive correlation with the active histone mark H3K4me3 and a significant association of *Nanog*'s interacting loci with Klf4 binding, further supporting its possible role in regulating long-range chromatin interactions (Figures 3D and 5G). Thus, forced expression of Oct4, Sox2, Klf4, and c-Myc induces reorganization of chromatin architecture and facilitates interactions of the *Nanog* locus with other Klf4 target genes, as well as with open chromatin domains.

Reprogramming Factors and Mediator Cooperate during the Establishment of *Nanog*-Centered Interactions

To investigate whether Mediator and cohesin are involved in the acquisition of pluripotency, we assayed the potential to generate iPSCs from reprogrammable MEFs when subunits of Mediator (Med1 and Med12) and/or cohesin (Smc1a, Smc3, and Rad21) were depleted (Figure S6A). Indeed, KD of Mediator and/or cohesin components significantly decreased reprogramming efficiencies (Figure 6A).

Upon KD of Mediator and cohesin components, fewer iPSC colonies could result from either deficient reprogramming or immediate differentiation of newly formed iPSCs. To distinguish between these possibilities, we analyzed early (SSEA1) and late (EpCam) markers of pluripotency at intermediate stages of reprogramming (Polo et al., 2012). We focused on *Med1* KD cells because Med1 is expressed most differentially between somatic and pluripotent cells (Figure S6B) (Kagey et al., 2010; Polo et al., 2012). Figure 6B shows that *Med1* KD MEFs gave rise to fewer SSEA1$^+$ and EpCam$^+$ reprogramming intermediates at day 9 of reprogramming-factor overexpression. 3C analysis at this time point showed that *Nanog* promoter-enhancer looping was not efficiently established in the absence of Med1, concordant with decreased transcription (Figure 6C). Together, these data suggest that Med1 is important for acquiring pluripotency-specific chromatin loops and gene expression in addition to its established role in the maintenance of pluripotency.

We hypothesized that Med1 might cooperate with reprogramming factors to reorganize 3D chromatin architecture and to control gene expression during iPSC formation. Coimmunoprecipitation experiments in piPSCs showed association of Med1 with the reprogramming factors Oct4, Sox2, and Klf4 (Figure 6D), as well as with Med12 and Smc1 (Figure S6C), which have previously been reported to interact with Med1 in ESCs (Borggrefe and Yue, 2011; Kagey et al., 2010). Importantly, these protein-protein interactions were detected as early as 48 hr after expression of the reprogramming factors, suggesting an early function. Med1's interactions with Oct4 and Sox2 were also confirmed in ESCs (Figure S6C). These results indicate that Mediator components and pluripotency factors form a multiprotein complex throughout cellular reprogramming and in pluripotent cells.

Lastly, we asked how reprogramming factors might collaborate with Mediator and/or cohesin to form chromatin loops during reprogramming. We investigated the binding of these proteins to three genomic regions (*Aicda*, *Nanog* enhancer, and *Slc2a3*) found to interact with the *Nanog* promoter in pluripotent cells based on m4C-seq data (Figure 6E). This analysis showed that Klf4, Oct4, Sox2, Med1, and Smc1 were bound to all three loci in pluripotent cells (Figure S6D). Similarly, the loci that had already established chromatin loops with the *Nanog* promoter (*Nanog* enhancer and *Slc2a3*) in piPSC lines were occupied by all tested factors (Figure 6F). In contrast, *Aicda*, which interacted with the *Nanog* promoter in established iPSCs only, but not yet in piPSCs, was bound solely by Klf4 in piPSCs. This result suggests that a minimum set of pluripotency proteins may be required by cohesin and Mediator to bridge distal chromatin elements.

DISCUSSION

Herein, we provide genetic, biochemical, and bioinformatic evidence that *Nanog* engages in a pluripotency-specific genome-wide chromatin network that resolves into a somatic-specific pattern upon differentiation and resets in iPSCs (Figure 7). This is the first genome-wide interaction map of a key mouse pluripotency gene at high resolution. Our results extend previous genome-scale transcription factor occupancy and protein interaction studies for pluripotency factors (Chen et al., 2008; Kim et al., 2008) and reveal an unexpectedly complex genomic interactome in pluripotent cells.

We document *Nanog* promoter interactions with individual loci as well as broader domains on the same and on different chromosomes. These interactions were stable and conserved among different pluripotent cell lines, whereas they were less consistent in MEFs (Figure 7). This finding indicates that pluripotency loci might engage in less stable and/or more random interactions in cell types wherein the bait locus is inactive. Alternatively, it may reflect the heterogeneity of fibroblast populations, which were used as a proxy for differentiated cells. Of note, almost half of the conserved interactions found in MEF samples were also detected in pluripotent cells, indicating a cell-type independent network of presumably structural interactions.

A positive correlation between *Nanog*-centered interactions and active chromatin marks specifically in pluripotent cells is in accordance with previous studies showing that active genes

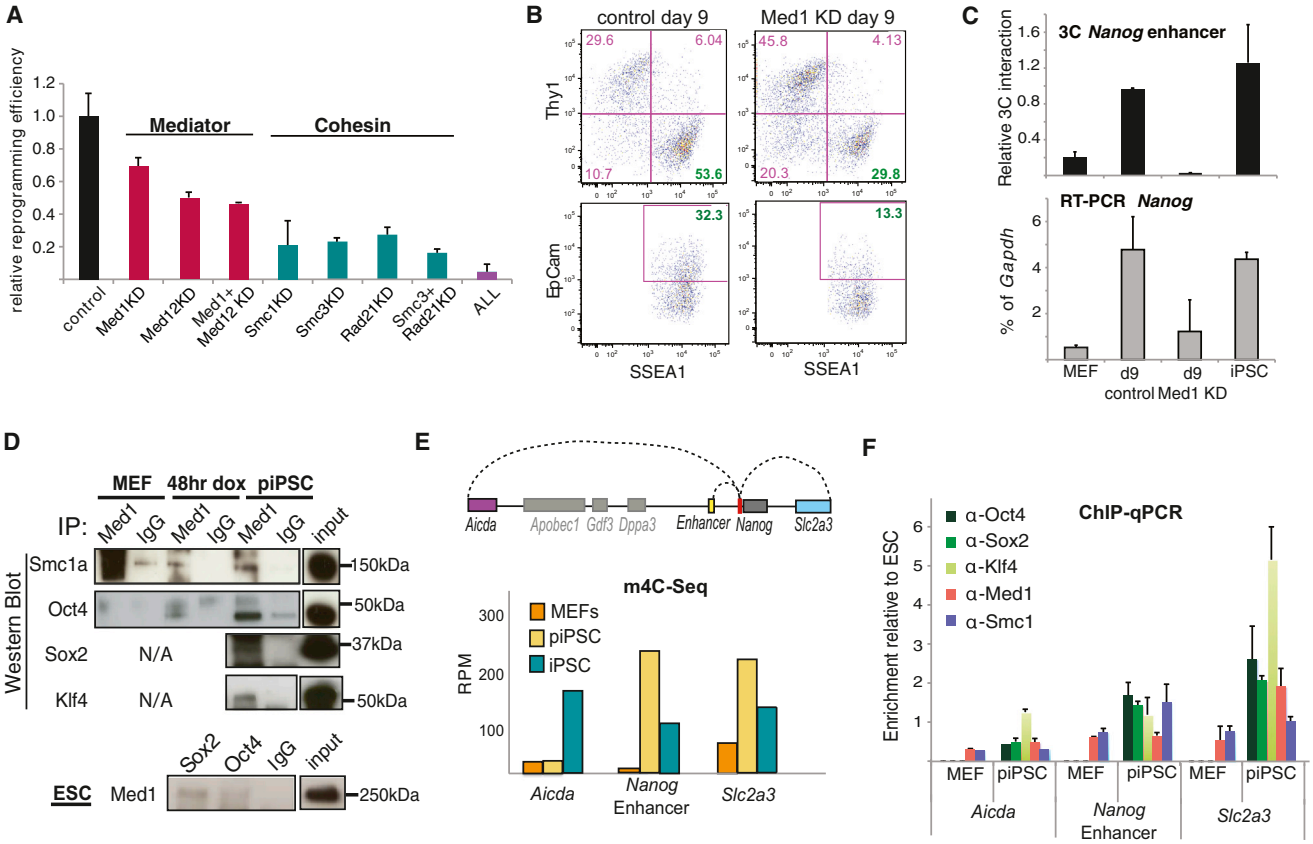

Figure 6. Role of Mediator and Cohesin in the Reprogramming of MEFs to iPSCs

(A) Graph comparing the reprogramming efficiency of tetO-OKSM MEFs after infection with empty vector (control) or shRNA vectors (KD) against individual subunits of Mediator (Med1 and Med12) or cohesin (Smc1a, Smc3, and Rad21) complexes or combinations thereof. The efficiency was calculated as the ratio of alkaline-phosphatase-positive colonies per starting number of cells. Reprogramming efficiency of control MEFs was set at 1. Error bars indicate SD (n = 3 biological replicates).

(B) Fluorescence-activated cell sorting plots of SSEA1-positive or EpCam-positive cells on day 9 of reprogramming, starting with either wild-type (left) or Med1-knocked down (KD, right) reprogrammable MEFs. SSEA1 and EpCam were chosen as early or late surface markers of pluripotency, respectively.

(C) RT-PCR (bottom) for *Nanog* expression and 3C assay (top) for *Nanog* enhancer-promoter interaction in MEFs, iPSCs, and reprogramming intermediates of control or Med1 KD MEFs on day 9. The 3C PCR signal was calculated relative to ESCs ("Relative 3C Interaction") after normalization with bait-locus primers (Table S6). Error bars represent SD (n = 2 technical replicates). The RT-PCR *Nanog* signal was normalized to *Gapdh* levels, and the error bars indicate SD (n = 4 replicates).

(D) Med1 protein immunoprecipitation (upper panels) in reprogrammable MEFs before (MEF) and after (MEF 48 hr) doxycycline induction and in piPSCs. In the bottom panel, the interaction of Med1 with Oct4, Sox2, and Nanog was also confirmed in ESCs, this time using antibodies for the reprogramming factors for the pull-down.

(E) Schematic representation of the genomic regions found to interact in *cis* with the *Nanog* promoter (red) in a pluripotent-specific way (top). Barplot of the m4C-seq signal for each of the indicated regions in MEFs, piPSCs, and ESCs. The signal is expressed in reads per million (RPM) and represents the average value of three biological replicates.

(F) ChIP experiments of the reprogramming factors Oct4, Sox2, and Klf4, as well as Med1 and Smc1a, on the indicated genomic regions in MEFs and piPSCs. All of the ChIP-qPCR signals are first normalized to the input, and then expressed relative to the corresponding signal in ESCs (see also Figure S6). Error bars indicate SD.

See also Figure S6 and Table S6.

tend to colocalize in the genome (Gao et al., 2013; Kalhor et al., 2012; Simonis et al., 2006). Notably, binding sites for the key pluripotency factors Oct4, Sox2, Nanog, Esrrb, c-Myc, and Klf4 were also enriched among the *Nanog*-interacting genes in pluripotent cells (Figure 7), suggesting that these proteins might be involved in bringing coregulated pluripotency-associated genes into physical proximity for subsequent transcriptional activation during the induction and maintenance of pluripotency. Indeed, previous studies documented roles for Oct4 in the maintenance of *cis* DNA loops around *Nanog* (Levasseur et al., 2008), for c-Myc in the spatial organization of ribosomal RNA genes in other cell types (Shiue et al., 2009), and for Klf1 in long-range interactions of erythroid genes during blood cell development (Schoenfelder et al., 2010). It is worth mentioning here that forced expression of either of c-Myc, Nanog, Esrrb, or Klf4 proteins relieves ESCs from leukemia-inhibitory-factor-dependent growth (Festuccia et al., 2012; Jiang et al., 2008; Marks et al., 2012; Smith and Dalton, 2010; Smith et al., 2010), suggesting

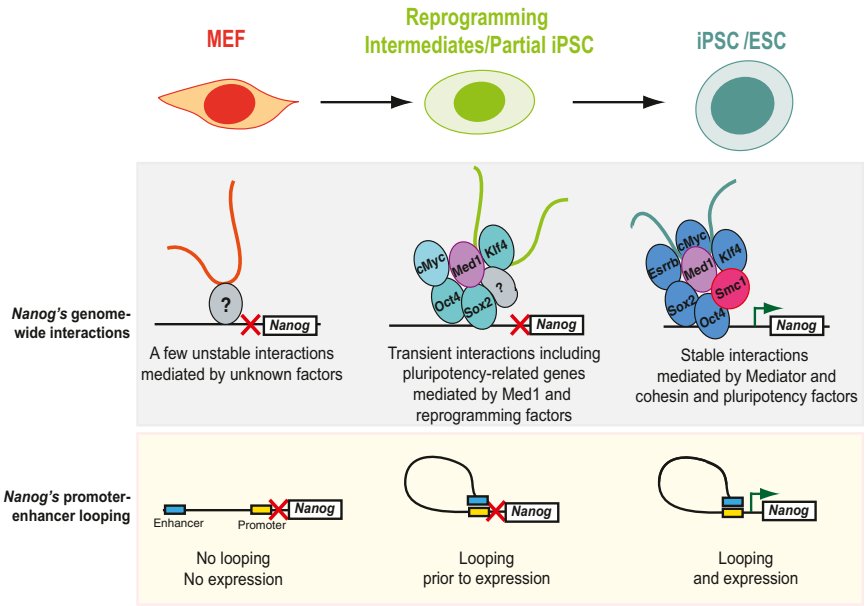

Figure 7. Model Depicting the Dynamics of *Nanog* Interactions during Differentiation and Cellular Reprogramming

The *Nanog* locus engages in genome-wide chromatin interactions in MEFs ("MEF-specific interactome") that are highly variable, possibly because the *Nanog* gene is inactive in differentiated cells. During reprogramming, the complexity of interactions increases, presumably by the cooperative action of the overexpressed reprogramming factors and "bridging" factors, including Mediator components (Med1). The majority of interactions gained in piPSCs lead to upregulation of associated genes immediately or in iPSCs. Once cells reach the pluripotent state, different and more-stable interactions are established. These pluripotency-specific interactions are mainly maintained by cohesin and Mediator complexes, as well as the key pluripotency factors. Upon normal differentiation or depletion of either Med1 or Smc1a, the *Nanog* interactome is rearranged into the less-organized differentiated state.

that the observed interaction network and its constituents may also be functionally connected.

We provide evidence that members of the Mediator and/or cohesin families are responsible for about 40% of the observed interactions in ESCs. Their depletion from ESCs resulted in a rearrangement of chromatin from a pluripotent to a differentiated state before the transcriptional and phenotypic onset of differentiation. Similarly, their reduction during cellular reprogramming impaired iPSC colony formation, suggesting an additional role in establishing pluripotency. Our observation that Med1 associated physically with the overexpressed Oct4, Sox2, and Klf4 factors during reprogramming and with the corresponding endogenous proteins in established ESCs supports this interpretation and extends previous results regarding the direct interactions of cohesin and Mediator subunits with Oct4 and Nanog in ESCs (Costa et al., 2013; Nitzsche et al., 2011; Tutter et al., 2009; van den Berg et al., 2010). Our results therefore suggest that Mediator and cohesin components, in collaboration with pluripotency transcription factors, play a critical role in establishing and maintaining a broader 3D chromatin network centered around *Nanog* and possibly other pluripotency loci (Figure 7). We cannot exclude the possibility that Mediator and cohesin influence iPSC formation and ESC maintenance by additional mechanisms such as cell cycle, cell signaling (Rocha et al., 2010), mesenchymal-to-epithelial transition (Huang et al., 2012), and/or transcriptional regulation (Malik and Roeder, 2010; Wood et al., 2010).

Lastly, we document that the reprogramming of somatic cells into iPSCs resets *Nanog*'s chromatin interactome. We show that fibroblasts rapidly lose MEF-specific interactions upon overexpression of Oct4, Sox2, Klf4, and c-Myc and gradually establish pluripotency-specific interactions. This is in accordance with the transcriptional shutdown of the somatic program prior to the activation of the pluripotency program as described recently (Polo et al., 2012; Soufi et al., 2012; Stadtfeld et al., 2008). Unexpectedly, we detected a number of transient, reprogramming-specific contacts, which involved many pluripotency-related genes (Figure 7). These genes might be physically brought together with *Nanog* by forced reprogramming-factor expression for coordinated gene activation. The observed protein-protein interactions of Oct4, Sox2, and Klf4 with Med1 in piPSCs support a model whereby reprogramming factors and associated bridging factors act synergistically to orchestrate chromatin rearrangements during reprogramming (Figure 7). However, we cannot rule out the possibility that these interactions might be the consequence of global chromatin changes or aberrant binding of the overexpressed transcription factors during reprogramming (Soufi et al., 2012).

Collectively, our data provide a comprehensive analysis of the genomic interactions of a key pluripotency gene and their relationship with transcription, epigenetic marks, and pluripotency-factor binding. Our findings further suggest an important and possibly causative role for chromatin structure in controlling transcriptional patterns and eventually determining cell identity in the context of pluripotency, differentiation, and cellular reprogramming. Identifying the interactomes for other pluripotency loci should allow researchers to construct an integrative view of 3D chromatin architecture in pluripotent cells in the future.

EXPERIMENTAL PROCEDURES

Cell Culture and Reprogramming

ESCs, MEF-derived iPSCs (Stadtfeld et al., 2010a), and piPSCs (Maherali et al., 2007) were cultured as described before. MEFs were isolated from "reprogrammable" mice (Stadtfeld et al., 2010b) and reprogrammed in presence of 1 μg/ml doxycycline and 50 μg/ml ascorbic acid.

shRNA Virus Production and Infection

The shRNA lentiviruses for Med1 and Smc1a were designed according to a previous study (Kagey et al., 2010) and cloned into a different vector (Addgene-pSicoR-GFP). The virus production, transduction, and reprogramming of infected MEFs are described in Supplemental Experimental Procedures. All the shRNA sequences used for this study are shown in Table S6.

RNA-Seq Library Preparation

The RNA-seq library construction is described in the Supplemental Experimental Procedures.

Protein Coimmunoprecipitation

The antibodies used for this study were as follows: Med1 (Bethyl Laboratories), Smc1 (Bethyl Laboratories), Oct4 (Santa Cruz Biotechnology for western blotting and R&D Systems for immunoprecipitation), Sox2 (R&D), Klf4 (R&D), Nanog (Bethyl Laboratories), actin-HPRT (Abcam), Med12 (Bethyl Laboratories), Smc3 (Abcam), and Rad21 (Santa Cruz). The exact process is described in the Supplemental Experimental Procedures.

ChIP

ChIP was performed as described previously (Stadtfeld et al., 2012). The antibodies used were as follows: Oct4 (R&D), Sox2 (R&D), Klf4 (R&D), Med1 (Bethyl Laboratories), Smc1 (Bethyl Laboratories), immunoglobulin G (Abcam), and Pol II phospho-Ser2 (Abcam). The primers used for the quantitative PCR (qPCR) analysis are listed in Table S6.

3D DNA FISH and Image Analysis

3D DNA FISH analysis was performed as described previously (Xu et al., 2006). The protocol and the bacterial artificial clones used for this study are listed in the Supplemental Experimental Procedures.

m4C-Seq, m4C-ChIP-Seq, and 3C Analyses

4C and 3C were performed as has been previously described (Schoenfelder et al., 2010) with some modifications, described in detail in the Supplemental Experimental Procedures. For m4C-ChIP-seq, an immunoprecipitation step with Med1 and Smc1 antibodies (Bethyl Laboratories) was included. The primers used for these assays are listed in Table S6.

Bioinformatics Analyses of m4C-Seq and Associations with Public Data Sets

See Supplemental Experimental Procedures.

ACCESSION NUMBERS

The Sequence Read Archive accession number for sequencing data reported in this paper is SRA051554.

SUPPLEMENTAL INFORMATION

Supplemental Information includes Supplemental Experimental Procedures, six figures, and six tables and can be found with this article online at http://dx.doi.org/10.1016/j.stem.2013.04.013.

ACKNOWLEDGMENTS

We acknowledge Peter Fraser, Frank Grosveld, Jane Skok, and Job Dekker for comments and suggestions. We thank Mariann Miscinai and Triantiafyllos Paparountas for discussing bioinformatics analysis, Eda Yildirim and Berni Peyer for advice about FISH experiments, and all members of the Hochedlinger and Park groups for suggestions. E.A. was supported by postdoctoral fellowships from JCCF and HHMI. P.J.P. was supported by a Sloan Research Fellowship and NIH (RC2HL102815), P.V.K was supported by NIH (K25AG037596), and K.H. was supported by NIH (DP2OD003266 and R01HD058013).

Received: April 11, 2012
Revised: March 27, 2013
Accepted: April 16, 2013
Published: May 9, 2013

REFERENCES

Apostolou, E., and Thanos, D. (2008). Virus Infection Induces NF-kappaB-dependent interchromosomal associations mediating monoallelic IFN-beta gene expression. Cell *134*, 85–96.

Bantignies, F., Roure, V., Comet, I., Leblanc, B., Schuettengruber, B., Bonnet, J., Tixier, V., Mas, A., and Cavalli, G. (2011). Polycomb-dependent regulatory contacts between distant Hox loci in Drosophila. Cell *144*, 214–226.

Borggrefe, T., and Yue, X. (2011). Interactions between subunits of the Mediator complex with gene-specific transcription factors. Semin. Cell Dev. Biol. *22*, 759–768.

Buganim, Y., Faddah, D.A., Cheng, A.W., Itskovich, E., Markoulaki, S., Ganz, K., Klemm, S.L., van Oudenaarden, A., and Jaenisch, R. (2012). Single-cell expression analyses during cellular reprogramming reveal an early stochastic and a late hierarchic phase. Cell *150*, 1209–1222.

Chambers, I., Colby, D., Robertson, M., Nichols, J., Lee, S., Tweedie, S., and Smith, A. (2003). Functional expression cloning of Nanog, a pluripotency sustaining factor in embryonic stem cells. Cell *113*, 643–655.

Chen, X., Xu, H., Yuan, P., Fang, F., Huss, M., Vega, V.B., Wong, E., Orlov, Y.L., Zhang, W., Jiang, J., et al. (2008). Integration of external signaling pathways with the core transcriptional network in embryonic stem cells. Cell *133*, 1106–1117.

Clowney, E.J., LeGros, M.A., Mosley, C.P., Clowney, F.G., Markenskoff-Papadimitriou, E.C., Myllys, M., Barnea, G., Larabell, C.A., and Lomvardas, S. (2012). Nuclear aggregation of olfactory receptor genes governs their monogenic expression. Cell *151*, 724–737.

Costa, Y., Ding, J., Theunissen, T.W., Faiola, F., Hore, T.A., Shliaha, P.V., Fidalgo, M., Saunders, A., Lawrence, M., Dietmann, S., et al. (2013). NANOG-dependent function of TET1 and TET2 in establishment of pluripotency. Nature *495*, 370–374.

Dekker, J., Rippe, K., Dekker, M., and Kleckner, N. (2002). Capturing chromosome conformation. Science *295*, 1306–1311.

Dixon, J.R., Selvaraj, S., Yue, F., Kim, A., Li, Y., Shen, Y., Hu, M., Liu, J.S., and Ren, B. (2012). Topological domains in mammalian genomes identified by analysis of chromatin interactions. Nature *485*, 376–380.

Donohoe, M.E., Silva, S.S., Pinter, S.F., Xu, N., and Lee, J.T. (2009). The pluripotency factor Oct4 interacts with Ctcf and also controls X-chromosome pairing and counting. Nature *460*, 128–132.

Duan, Z., Andronescu, M., Schutz, K., McIlwain, S., Kim, Y.J., Lee, C., Shendure, J., Fields, S., Blau, C.A., and Noble, W.S. (2010). A three-dimensional model of the yeast genome. Nature *465*, 363–367.

ENCODE Project Consortium. (2011). A user's guide to the encyclopedia of DNA elements (ENCODE). PLoS Biol. *9*, e1001046.

Engel, J.D., and Tanimoto, K. (2000). Looping, linking, and chromatin activity: new insights into beta-globin locus regulation. Cell *100*, 499–502.

Festuccia, N., Osorno, R., Halbritter, F., Karwacki-Neisius, V., Navarro, P., Colby, D., Wong, F., Yates, A., Tomlinson, S.R., and Chambers, I. (2012). Esrrb is a direct Nanog target gene that can substitute for Nanog function in pluripotent cells. Cell Stem Cell *11*, 477–490.

Gao, F., Wei, Z., An, W., Wang, K., and Lu, W. (2013). The interactomes of POU5F1 and SOX2 enhancers in human embryonic stem cells. Sci. Rep. *3*, 1588.

Golipour, A., David, L., Liu, Y., Jayakumaran, G., Hirsch, C.L., Trcka, D., and Wrana, J.L. (2012). A late transition in somatic cell reprogramming requires regulators distinct from the pluripotency network. Cell Stem Cell *11*, 769–782.

Hiratani, I., Ryba, T., Itoh, M., Yokochi, T., Schwaiger, M., Chang, C.-W., Lyou, Y., Townes, T.M., Schübeler, D., and Gilbert, D.M. (2008). Global reorganization of replication domains during embryonic stem cell differentiation. PLoS Biol. *6*, e245.

Hiratani, I., Ryba, T., Itoh, M., Rathjen, J., Kulik, M., Papp, B., Fussner, E., Bazett-Jones, D.P., Plath, K., Dalton, S., et al. (2010). Genome-wide dynamics of replication timing revealed by in vitro models of mouse embryogenesis. Genome Res. *20*, 155–169.

Huang, S., Hölzel, M., Knijnenburg, T., Schlicker, A., Roepman, P., McDermott, U., Garnett, M., Grernrum, W., Sun, C., Prahallad, A., et al. (2012). MED12 controls the response to multiple cancer drugs through regulation of TGF-β receptor signaling. Cell *151*, 937–950.

Jiang, J., Chan, Y.S., Loh, Y.H., Cai, J., Tong, G.Q., Lim, C.A., Robson, P., Zhong, S., and Ng, H.H. (2008). A core Klf circuitry regulates self-renewal of embryonic stem cells. Nat. Cell Biol. *10*, 353–360.

Kagey, M.H., Newman, J.J., Bilodeau, S., Zhan, Y., Orlando, D.A., van Berkum, N.L., Ebmeier, C.C., Goossens, J., Rahl, P.B., Levine, S.S., et al. (2010). Mediator and cohesin connect gene expression and chromatin architecture. Nature *467*, 430–435.

Kalhor, R., Tjong, H., Jayathilaka, N., Alber, F., and Chen, L. (2012). Genome architectures revealed by tethered chromosome conformation capture and population-based modeling. Nat. Biotechnol. *30*, 90–98.

Kim, J., Chu, J., Shen, X., Wang, J., and Orkin, S.H. (2008). An extended transcriptional network for pluripotency of embryonic stem cells. Cell *132*, 1049–1061.

Klein, I.A., Resch, W., Jankovic, M., Oliveira, T., Yamane, A., Nakahashi, H., Di Virgilio, M., Bothmer, A., Nussenzweig, A., Robbiani, D.F., et al. (2011). Translocation-capture sequencing reveals the extent and nature of chromosomal rearrangements in B lymphocytes. Cell *147*, 95–106.

Levasseur, D.N., Wang, J., Dorschner, M.O., Stamatoyannopoulos, J.A., and Orkin, S.H. (2008). Oct4 dependence of chromatin structure within the extended Nanog locus in ES cells. Genes Dev. *22*, 575–580.

Lieberman-Aiden, E., van Berkum, N.L., Williams, L., Imakaev, M., Ragoczy, T., Telling, A., Amit, I., Lajoie, B.R., Sabo, P.J., Dorschner, M.O., et al. (2009). Comprehensive mapping of long-range interactions reveals folding principles of the human genome. Science *326*, 289–293.

Ling, J.Q., Li, T., Hu, J.F., Vu, T.H., Chen, H.L., Qiu, X.W., Cherry, A.M., and Hoffman, A.R. (2006). CTCF mediates interchromosomal colocalization between Igf2/H19 and Wsb1/Nf1. Science *312*, 269–272.

Lomvardas, S., Barnea, G., Pisapia, D.J., Mendelsohn, M., Kirkland, J., and Axel, R. (2006). Interchromosomal interactions and olfactory receptor choice. Cell *126*, 403–413.

Maherali, N., Sridharan, R., Xie, W., Utikal, J., Eminli, S., Arnold, K., Stadtfeld, M., Yachechko, R., Tchieu, J., Jaenisch, R., et al. (2007). Directly reprogrammed fibroblasts show global epigenetic remodeling and widespread tissue contribution. Cell Stem Cell *1*, 55–70.

Malik, S., and Roeder, R.G. (2010). The metazoan Mediator co-activator complex as an integrative hub for transcriptional regulation. Nat. Rev. Genet. *11*, 761–772.

Marks, H., Kalkan, T., Menafra, R., Denissov, S., Jones, K., Hofemeister, H., Nichols, J., Kranz, A., Stewart, A.F., Smith, A., and Stunnenberg, H.G. (2012). The transcriptional and epigenomic foundations of ground state pluripotency. Cell *149*, 590–604.

Mikkelsen, T.S., Hanna, J., Zhang, X., Ku, M., Wernig, M., Schorderet, P., Bernstein, B.E., Jaenisch, R., Lander, E.S., and Meissner, A. (2008). Dissecting direct reprogramming through integrative genomic analysis. Nature *454*, 49–55.

Mitsui, K., Tokuzawa, Y., Itoh, H., Segawa, K., Murakami, M., Takahashi, K., Maruyama, M., Maeda, M., and Yamanaka, S. (2003). The homeoprotein Nanog is required for maintenance of pluripotency in mouse epiblast and ES cells. Cell *113*, 631–642.

Nitzsche, A., Paszkowski-Rogacz, M., Matarese, F., Janssen-Megens, E.M., Hubner, N.C., Schulz, H., de Vries, I., Ding, L., Huebner, N., Mann, M., et al. (2011). RAD21 cooperates with pluripotency transcription factors in the maintenance of embryonic stem cell identity. PLoS ONE *6*, e19470.

Peric-Hupkes, D., Meuleman, W., Pagie, L., Bruggeman, S.W., Solovei, I., Brugman, W., Gräf, S., Flicek, P., Kerkhoven, R.M., van Lohuizen, M., et al. (2010). Molecular maps of the reorganization of genome-nuclear lamina interactions during differentiation. Mol. Cell *38*, 603–613.

Polo, J.M., Anderssen, E., Walsh, R.M., Schwarz, B.A., Nefzger, C.M., Lim, S.M., Borkent, M., Apostolou, E., Alaei, S., Cloutier, J., et al. (2012). A molecular roadmap of reprogramming somatic cells into iPS cells. Cell *151*, 1617–1632.

Rocha, P.P., Scholze, M., Bleiss, W., and Schrewe, H. (2010). Med12 is essential for early mouse development and for canonical Wnt and Wnt/PCP signaling. Development *137*, 2723–2731.

Rocha, P.P., Micsinai, M., Kim, J.R., Hewitt, S.L., Souza, P.P., Trimarchi, T., Strino, F., Parisi, F., Kluger, Y., and Skok, J.A. (2012). Close proximity to Igh is a contributing factor to AID-mediated translocations. Mol. Cell *47*, 873–885.

Schardin, M., Cremer, T., Hager, H.D., and Lang, M. (1985). Specific staining of human chromosomes in Chinese hamster x man hybrid cell lines demonstrates interphase chromosome territories. Hum. Genet. *71*, 281–287.

Schoenfelder, S., Sexton, T., Chakalova, L., Cope, N.F., Horton, A., Andrews, S., Kurukuti, S., Mitchell, J.A., Umlauf, D., Dimitrova, D.S., et al. (2010). Preferential associations between co-regulated genes reveal a transcriptional interactome in erythroid cells. Nat. Genet. *42*, 53–61.

Sexton, T., Yaffe, E., Kenigsberg, E., Bantignies, F., Leblanc, B., Hoichman, M., Parrinello, H., Tanay, A., and Cavalli, G. (2012). Three-dimensional folding and functional organization principles of the Drosophila genome. Cell *148*, 458–472.

Shiue, C.N., Berkson, R.G., and Wright, A.P. (2009). c-Myc induces changes in higher order rDNA structure on stimulation of quiescent cells. Oncogene *28*, 1833–1842.

Silva, J., Nichols, J., Theunissen, T.W., Guo, G., van Oosten, A.L., Barrandon, O., Wray, J., Yamanaka, S., Chambers, I., and Smith, A. (2009). Nanog is the gateway to the pluripotent ground state. Cell *138*, 722–737.

Simonis, M., Klous, P., Splinter, E., Moshkin, Y., Willemsen, R., de Wit, E., van Steensel, B., and de Laat, W. (2006). Nuclear organization of active and inactive chromatin domains uncovered by chromosome conformation capture-on-chip (4C). Nat. Genet. *38*, 1348–1354.

Simonis, M., Klous, P., Homminga, I., Galjaard, R.-J., Rijkers, E.-J., Grosveld, F., Meijerink, J.P., and de Laat, W. (2009). High-resolution identification of balanced and complex chromosomal rearrangements by 4C technology. Nat. Methods *6*, 837–842.

Smith, K., and Dalton, S. (2010). Myc transcription factors: key regulators behind establishment and maintenance of pluripotency. Regen. Med. *5*, 947–959.

Smith, K.N., Singh, A.M., and Dalton, S. (2010). Myc represses primitive endoderm differentiation in pluripotent stem cells. Cell Stem Cell *7*, 343–354.

Soufi, A., Donahue, G., and Zaret, K.S. (2012). Facilitators and impediments of the pluripotency reprogramming factors' initial engagement with the genome. Cell *151*, 994–1004.

Sridharan, R., Tchieu, J., Mason, M.J., Yachechko, R., Kuoy, E., Horvath, S., Zhou, Q., and Plath, K. (2009). Role of the murine reprogramming factors in the induction of pluripotency. Cell *136*, 364–377.

Stadtfeld, M., Maherali, N., Breault, D.T., and Hochedlinger, K. (2008). Defining molecular cornerstones during fibroblast to iPS cell reprogramming in mouse. Cell Stem Cell *2*, 230–240.

Stadtfeld, M., Apostolou, E., Akutsu, H., Fukuda, A., Follett, P., Natesan, S., Kono, T., Shioda, T., and Hochedlinger, K. (2010a). Aberrant silencing of imprinted genes on chromosome 12qF1 in mouse induced pluripotent stem cells. Nature *465*, 175–181.

Stadtfeld, M., Maherali, N., Borkent, M., and Hochedlinger, K. (2010b). A reprogrammable mouse strain from gene-targeted embryonic stem cells. Nat. Methods *7*, 53–55.

Stadtfeld, M., Apostolou, E., Ferrari, F., Choi, J., Walsh, R.M., Chen, T., Ooi, S.S., Kim, S.Y., Bestor, T.H., Shioda, T., et al. (2012). Ascorbic acid prevents loss of Dlk1-Dio3 imprinting and facilitates generation of all-iPS cell mice from terminally differentiated B cells. Nat. Genet. *44*, 398–405, S1–S2.

Takahashi, K., and Yamanaka, S. (2006). Induction of pluripotent stem cells from mouse embryonic and adult fibroblast cultures by defined factors. Cell *126*, 663–676.

Tutter, A.V., Kowalski, M.P., Baltus, G.A., Iourgenko, V., Labow, M., Li, E., and Kadam, S. (2009). Role for Med12 in regulation of Nanog and Nanog target genes. J. Biol. Chem. *284*, 3709–3718.

van den Berg, D.L., Snoek, T., Mullin, N.P., Yates, A., Bezstarosti, K., Demmers, J., Chambers, I., and Poot, R.A. (2010). An Oct4-centered protein interaction network in embryonic stem cells. Cell Stem Cell *6*, 369–381.

Wood, A.J., Severson, A.F., and Meyer, B.J. (2010). Condensin and cohesin complexity: the expanding repertoire of functions. Nat. Rev. Genet. *11*, 391–404.

Xu, N., Tsai, C.-L., and Lee, J.T. (2006). Transient homologous chromosome pairing marks the onset of X inactivation. Science *311*, 1149–1152.

Zhang, Y., McCord, R.P., Ho, Y.J., Lajoie, B.R., Hildebrand, D.G., Simon, A.C., Becker, M.S., Alt, F.W., and Dekker, J. (2012). Spatial organization of the mouse genome and its role in recurrent chromosomal translocations. Cell *148*, 908–921.

Zhao, Z., Tavoosidana, G., Sjölinder, M., Göndör, A., Mariano, P., Wang, S., Kanduri, C., Lezcano, M., Sandhu, K.S., Singh, U., et al. (2006). Circular chromosome conformation capture (4C) uncovers extensive networks of epigenetically regulated intra- and interchromosomal interactions. Nat. Genet. *38*, 1341–1347.